Published in final edited form as:
Biochim Biophys Acta. 2013 March ; 1830(3): 2600–2607. doi:10.1016/j.bbagen.2012.11.021.

The proteolytic processing of amelogenin by enamel matrix metalloproteinase (MMP-20) is controlled by mineral ions

Feroz Khan[a,1], **Haichuan Liu**[b], **Aileen Reyes**[a], **H. Ewa Witkowska**[b], **Olga Martinez-Avila**[a], **Li Zhu**[c], **Wu Li**[c], and **Stefan Habelitz**[a,*]

[a]Division of Biomaterials and Bioengineering, Department of Preventive and Restorative Dental Sciences, University of California, 707 Parnassus Avenue, San Francisco, CA 94143, USA

[b]Department of Obstetrics, Gynecology & Reproductive Sciences and UCSF Sandler-Moore Mass Spectrometry Core Facility, University of California, 521 Parnassus Avenue, San Francisco, CA 94143, USA

[c]Department of Orofacial Sciences, University of California, 513 Parnassus Avenue, San Francisco, CA 94143, USA

Abstract

Background—Enamel synthesis is a highly dynamic process characterized by simultaneity of matrix secretion, assembly and processing during apatite mineralization. MMP-20 is the first protease to hydrolyze amelogenin, resulting in specific cleavage products that self-assemble into nanostructures at specific mineral compositions and pH. In this investigation, enzyme kinetics of MMP-20 proteolysis of recombinant full-length human amelogenin (rH174) under different mineral compositions is elucidated.

Methods—Recombinant amelogenin was cleaved by MMP-20 under various physicochemical conditions and the products were analyzed by SDS-PAGE and MALDI-TOF MS.

Results—It was observed that mineral ions largely affect cleavage pattern, and enzyme kinetics of rH174 hydrolysis. Out of the five selected mineral ion compositions, MMP-20 was most efficient at high calcium concentration, whereas it was slowest at high phosphate, and at high calcium and phosphate concentrations. In most of the compositions, N- and C-termini were cleaved rapidly at several places but the central region of amelogenin was protected up to some extent in solutions with high calcium and phosphate contents.

Conclusion—These *in vitro* studies showed that the chemistry of the protein solutions can significantly alter the processing of amelogenin by MMP-20, which may have significant effects *in vivo* matrix assembly and subsequent calcium phosphate mineralization.

General significance—This study elaborates the possibilities of the processing of the organic matrix into mineralized tissue during enamel development.

*Corresponding author at: Division of Biomaterials and Bioengineering, Department of Preventive and Restorative Dental Sciences, University of California, Parnassus Avenue 707, San Francisco, CA 94143, USA. Tel.: +1 415 514 0818; fax: +1 415 476 0858. stefan.habelitz@ucsf.edu (S. Habelitz).
[1]Current address: Dr. D.Y. Patil Biotechnology & Bioinformatics Institute, Tathawade, Pune 411033, India.

Keywords

Enamelysin; Amelogenin; Enamel; Tooth; Proteolysis; Enzyme kinetics

1. Introduction

Amelogenesis is a remarkably dynamic process involving a series of biochemical processes, such as alternative splicing, secretion of several matrix proteins followed by self-assembly, biomineralization and simultaneous selective proteolysis culminating in the removal of the organic matter [1]. In this series of the events, amelogenin, the major constituent of organic enamel matrix, plays the most important role by self-assembling into supramolecular structures and scaffolding the growing enamel crystals [2]. Hitherto, the process of mineralization *via* self-assembled nanospheres remained largely enigmatic. The synthesis of amelogenin nanoribbons first in an artificial water–oil system [3] and recently in aqueous and near physiological conditions [4], has paved a way for the possibilities of *in vitro* synthesis of enamel like materials [5]. Amelogenin ribbons were formed in mineralizing solutions only upon addition of both of the calcium and phosphate ions to the amelogenin suspensions at pH between 4 and 6 [4]. Extensive aggregation of amelogenins (rH174, rH163 and rH146) with the particle size reaching about 1 μm was observed at a mildly acidic to neutral pH, and coincided with the red shift of the internal fluorescence [6].

The site-specific protease MMP-20 (matrix metalloproteinase; enamelysin) is expressed in early to mid-stages of the secretory phase of amelogenesis, and during this phase the enamel matrix proteins are processed in a stepwise fashion [7]. Several proteolytic products of amelogenin such as 23 kDa (rH163), 20 kDa (rH146), 13 kDa and TRAPs, have been reported so far during the post-secretory phase [1,8–11]. A second protease, Kalikrein-4 (KLK-4), is also expressed during maturation stage, after complete secretion of the enamel matrix proteins. Proper functioning of both, MMP-20 and KLK-4, is critical for correct dental enamel formation [12,13]. The knockout mice with disrupted MMP-20 produce enamel with lower thickness (~30 μm) and lower hardness (about 50%), while KLK-4 null mice develop the enamel crown of almost full width, but of low quality due to a high residual content of organic matrix [12,13].

The full length amelogenin is transiently present in the enamel matrix, and it is quickly processed to generate wide range of relatively smaller fragments [14]. MMP-20 is considered to have a regulatory role on functionality of amelogenins due to its high specificity for enamel matrix proteins [15]. There is some evidence suggesting that the cleavage products carry out different secondary self-assembly related functions in developing enamel matrix [14]. It was further established that the mixtures of full length amelogenin (rH174) and the proteolytic cleavage product (rH163) formed complex chain-like protein assemblies from the initial nanospheres with a remarkably higher propensity than the rH174 alone did [16]. Thus, it appears that amelogenin has a modular structure containing several domains that can be turned on by the action of MMP-20 and KLK-4 to carry out various functions at different stages of amelogenesis [17]. This notion is supported by the fact that MMP-20 is expressed early during tooth development [14] and some patients suffering from *Amelogenesis Imperfecta* (AI) also carried a novel MMP-20 mutation,

associated with the development of clinical symptoms [18]. Moreover, the postulated *in vivo* role of MMP-20 is strengthened by the fact that the *Mmp*-20-null mice are characterized by an altered enamel matrix and rod pattern with hypoplastic enamel that easily delaminates from the dentin [19].

MMP-20 belongs to a superfamily of metal dependent endo-peptidases involved in various tissue modeling processes such as embryonic development, wound healing, postpartum involution of the uterus, bone and growth plate remodeling; as well as degradation processes and pathological conditions such as arthritis, atherosclerosis, periodontitis, pulmonary emphysema, and tumor invasion and metastasis [20]. MMP-20 carries the characteristic domains of metalloproteinases –a signal peptide, a propeptide domain that maintains enzyme latency, a catalytic domain, and C-terminal hemopexin domain [14]. However, MMP-20 differs from other metalloproteinases as its expression is highly tooth-specific [21]; the conserved N-linked glycosylation is absent [7]; the hemopexin domain does not contain the consensus sequence [22]; and the unique hinge region is absent [23].

MMPs-20 have been cloned from the tooth-specific porcine [22], human [7] and bovine [24] cDNA libraries. Human MMP-20 has been cloned from cDNA isolated from odontoblastic cells. The open reading frame of the cloned cDNA codes for a polypeptide of 483 amino acids with a molecular mass of 54 kDa [7]. The recombinant MMPs-20 cleave amelogenin *in vitro* into several fragments under optimum physiological conditions [25,26]. However, differences in the cleavage pattern were reported for amelogenin and MMP-20 from different species [26]. The recombinant porcine MMP-20 cleaved recombinant murine amelogenin into a large number of smaller fragments when compared to the recombinant porcine amelogenin [26]. In another instance, when compared to the recombinant bovine MMP-20, the recombinant human MMP-20 showed higher enzymatic activity and produced more cleavage sites for human amelogenin under the conditions used in the study [25].

The apatite binding affinity of amelogenin was progressively reduced after the removal of C- and N-termini by MMP-20 and KLK4 [27]. The effect of apatite on the activity of MMP-20 and KLK4 was also explored and it was found that apatite reduces the rate of amelogenin proteolysis by MMP-20 and KLK4 [28]. Hydrolysis of amelogenin by MMP-20 during *in vitro* crystal growth of calcium phosphate crystals reduced the nucleation lag time in a concentration dependent manner indicating that *in situ* cleavage of full-length amelogenin accelerated mineralization [29].

It was reported earlier that the self-assembly of amelogenins leading to the formation of nanoribbons is largely affected by pH and mineral ion concentration [3,4], but it remained unclear if these conditions also affect its cleavage by MMP-20, which is the subject of this study. Recombinant human MMP-20 (rHMMP-20) was used to cleave the substrate – full length recombinant human amelogenin (rH174); and the various products, generated during the cleavage, were resolved by SDS-PAGE. Considering the initial amount of the substrate, the rate of the substrate cleavage was determined under various mineral ion compositions and subjected to Michaelis–Menten kinetics. Various cleavage patterns and site preferences were identified by MALDI TOF and tandem MS/MS analysis.

2. Materials and methods

2.1. Purification of recombinant proteins

Recombinant human amelogenins (rH174, rH163 and rH146) were expressed in *E. coli* BL21 (DE3) pLysS and purified on C4 hydrophobic beads as described earlier [30]. Human MMP-20 was also expressed in *Escherichia coli* BL21 (DE3) pLysS, purified using a nickel resin (ProBond, Life Technologies, Grand Island, USA) and activated by a stepwise dialysis against decreasing amounts of urea; and protease activity was determined by SDS-PAGE zymography [25]. The purity of the protein batches was above 95% as assessed by HPLC and SDS-PAGE (data not shown).

2.2. Enzyme kinetics

Substrate cleavage kinetics was monitored as time-dependent changes in the concentration of the amelogenin (rH174) under steady-state conditions (substrate/enzyme ratios of 15–940 folds). Various concentrations of the substrate (rH174) (2.5, 5.05, 12.6, 25.2, 50.5, 101, and 151 μM) were incubated with the enzyme (MMP-20) (0.16 μM) at 37 °C in a reaction buffer consisting of 10 mM Tris, 50 mM KCl, 1 μM $ZnCl_2$, and 60 μM $CaCl_2$ at pH 7.4. At various time intervals (0, 0.25, 0.5, 0.75, 1, 2, 3, 4, and 5 h), aliquots (3–6 μL) were withdrawn, mixed with 10 μL of SDS-PAGE loading buffer and immediately boiled for 10 min to stop the reaction. After completing the time-course experiment, samples were analyzed on 12.5% SDS-PAGE and protein bands were visualized by Coomassie brilliant blue R-250. Protein band intensity was measured using NIH software ImageJ 1.44p available at http://imagej.nih.gov/ij. The substrate (rH174) and product (rH163 and rH146) concentrations at different time points were normalized to the intensity of the full-length amelogenin (rH174) band representing the amount of the substrate loaded on the gel at time zero. The calibration curve was generated by measuring the intensities of bands corresponding to varying amounts of rH174 amelogenin loaded onto a SDS PAGE gel. Initial velocity v_0 was calculated from the slope of progress curve at time zero. Data from three independent sets of experiments were fitted to the Michaelis–Menten equation by non-linear regression. The experiments were carried out under the following sets of conditions: (a) *No Calcium and Phosphates* (Ca^{2+} and $H_xPO_4^{x-3}$) –only reaction buffer mentioned above (still contains 60 μM $CaCl_2$), (b) *Low Calcium and Phosphates* – the reaction buffer mentioned above with additional 3.34 mM $CaCl_2$ and 2.09 mM KH_2PO_4; (c) *High Calcium and Phosphates* – the reaction buffer mentioned above with additional 33.4 mM $CaCl_2$ and 20.9 mM KH_2PO_4; (d) *High Calcium* – the reaction buffer mentioned above with additional 33.4 mM $CaCl_2$; and (e) *High Phosphates* – the reaction buffer mentioned above with additional 20.9 mM KH_2PO_4 (addressing to these mineral compositions are capitalized and *italicized* throughout the manuscript to distinguish from general expressions addressing calcium and phosphates).

The first order reaction rate constant (k) was determined by the equation

$$\ln [S] = -kt + \ln [S]_0$$

and $T_{1/2}$ was determined by the equation

$$T_{1/2} = \ln(2)/k.$$

2.3. Mass spectrometry analysis

All mass spectrometric analyses were carried out on a 4800 MALDI-TOF/TOF mass spectrometer (AB Sciex, Foster City, CA) equipped with Nd:YAG LASER in either linear (m/z 1800–30,000) or reflector (m/z 800–6000) positive ion mode. For MALDI MS analyses, samples were desalted using ZipTip C18 (Millipore, Billerica, MA), and then were mixed 1:1 (v/v) directly on a 384-well MALDI stainless steel target (AB Sciex) with 5 mg/mL α-cyano-4-hydroxycinnamic acid (CHCA) in 80% acetonitrile (ACN)/0.1% trifluoroacetic acid (TFA)/10 mM dibasic ammonium phosphate. [Glu^1]-Fibrinopeptide B (m/z 1570.677 Da), at a concentration of 40 fmol/μL, was spiked into the MALDI matrix as standard for internal mass calibration. The off-line LC peptide fractionation was carried out on an Ultimate 3000 (Dionex, Sunnyvale, CA) LC system and employed a monolithic column (200 μm I.D., 5 cm length; Dionex). A 20-minute gradient, in percentage of Phase B (80% ACN/0.05% TFA) was linearly increased from 0% to 80% at flow rate of 2.5 μL/min. The eluted peptides were mixed with the matrix and spotted onto a blank MALDI target using a SunCollect spotter (SunChrom, Friedrichsdorf, Germany). MS and MS/MS data were acquired using 4000 Series Explorer software (AB Sciex). Peptides were identified by matching the MS/MS data against all human proteins in SwissProt database (release of 05/09/2011) with an aid of ProteinPilot™ Software 4.0 (Revision 148085). The following search parameters were used: digestion: none; instrument: 4800; ID focus: biological modifications and amino acid substitutions; search effort: thorough; and detected protein threshold [Unused ProtScore (Conf)>0.47] (66.00%). The majority of peptide identities reported here was matched by a search engine with a confidence above 99%. The peptides matched with confidence lower than 99% were accepted after manual inspection and verification of their MS/MS spectra.

2.4. Particle size measurements

Particle sizes of the proteins were measured by dynamic light scattering using a Zetasizer Nano (Malvern, UK) operating at a measurement range of 0.6 nm to 6 μm. The rH174 (1 mg/mL, *i.e.* 50.5 μM) and MMP-20 (0.16 μM) in the reaction buffers containing various mineral ions as described above were incubated in the Zetasizer at 37 °C and particle size was measured at 2-minute intervals. Particle size measured prior to addition of MMP-20 was considered as a time zero value.

3. Results

3.1. Effect of mineral ions on cleavage rate and pattern

An evaluation of effects of calcium and phosphates (Ca^{2+} and $H_xPO_4^{x-3}$) was carried out using five different compositions of mineral ions (see Materials and methods) (Fig. 1). All these studies were carried out only at pH 7.4 where MMP-20 shows maximum activity, and for a relevant comparison of the data reported by others [25,26,28].

The cleavage rate was accelerated in *High Calcium* and slowed down in *High Calcium and Phosphates* composition (Fig. 1D and C). The substrate cleavage rate seemed to be directly related to the concentrations of calcium and phosphate ions and it decreased in the follow order: *No Calcium and Phosphates>Low Calcium and Phosphates> High Calcium and Phosphates*.

The effect of calcium and phosphate ion concentrations was not limited to the cleavage rate but also appeared to influence the cleavage pattern. Under the *No Calcium and Phosphates* conditions, a preference for the site P^{163} was demonstrated by an accumulation of rH163 over time (Fig. 1A). However, this trend did not show any relation to the concentration of mineral ions. At the *Low Calcium and Phosphates* composition, the site preference was extremely weak (Fig. 1B). In contrast, under the *High Calcium and Phosphates* conditions, the preferences for the P^{163} and P^{146} sites were prominent, as depicted in Fig. 1C by the accumulation of rH163 and rH146, respectively. Under the latter conditions, the plot for initial activity was closer to linearity, which indicates a monophasic cleavage reaction, where no other sites seem to be cleaved except these two at an initial timescale.

Striking differences were observed in the *High Calcium* composition, where fastest cleavage rate was observed with a complete loss of site preference. In contrast, *High Phosphates* showed exclusive preference for P^{163} site as seen by the linear accumulation of rH163 (Fig. 1E). The substrate cleavage rate remained linear up to 5 h indicating monophasic cleavage kinetics.

3.2. Effect of mineral ions on enzyme kinetics

The initial reaction velocities for seven different substrate concentrations were fitted to Michaelis–Menten equation under steady state conditions, where substrate concentration remained 15–940 times higher than the enzyme. The Michaelis–Menten plots are shown in Fig. 2 and the obtained kinetic parameters are given in Table 1. The maximum reaction velocity (V_{max}) was obtained at the *High Calcium* composition (Fig. 2D) (V_{max} =7.5 μM/min) which was 11–25 folds higher than that observed for other compositions. However, this increase in V_{max} was also accompanied by K_m increase (K_m=584.6 μM), indicating that in spite of an increase in the reaction velocity, the enzyme–substrate affinity declined. Among all the compositions, *High Calcium and Phosphates* showed minimum V_{max} (0.30 μM/min) and K_m (19.51 μM) (Fig. 2C and Table 1).

The turnover number (K_{cat}) was also found to be the highest for the *High Calcium* composition indicating that the enzyme works fastest at this condition (11–24 times higher than that observed for other compositions). However, it is interesting to note that enzyme efficiency (K_{cat}/K_m) does not follow the same trend. MMP-20 showed maximum efficiency in *No Calcium and Phosphates* composition ($K_{cat}/K_m = 1.9\times10^3$ M^{-1} s^{-1}) contrary to what was observed for V_{max} (Fig. 2A and Table 1). The efficiency was equal ($K_{cat}/K_m =1.6\times10^3$ M^{-1} s^{-1}) under more physiologically relevant conditions of *Low Calcium and Phosphates* and *High Calcium and Phosphates*, where both mineral ions are present (Fig. 2B and C and Table 1). However, enzyme efficiency was lowest ($K_{cat}/K_m =0.8\times10^3$ M^{-1} s^{-1}) at *High Phosphates* composition (Table 1 and Fig. 2E).

The rate constants (k) and half life ($T_{1/2}$) were higher at the *High Calcium* (k=32.9×10^{-5}1/s, $T_{1/2}$ =35 min), *No Calcium and Phosphates* (k=24.5×10^{-5}1/s, $T_{1/2}$=47 min), and *Low Calcium and Phosphates* (k=15.8×10^{-5}1/s, $T_{1/2}$ =73 min) compositions, and lower at *High Calcium and Phosphates* (k=5.01×10^{-5}1/s, $T_{1/2}$ =227 min) and the *High Phosphates* (k=3.21×10^{-5}1/s, $T_{1/2}$=370 min) (Table 1), in relation to their respective V_{max}.

3.3. Effect of mineral ions on cleavage sites

The peptides generated during the proteolyses were identified by LC MS/MS, and based on their sequences, the cleavage sites within rH174 were derived, as shown in Fig. 3. Variations in the preference for the cleavage sites were observed in all the compositions used. Some sites were cleaved specifically under certain conditions with an apparent time lag in the appearance of certain fragments. In all compositions, amelogenin was initially cleaved only at the terminal regions, and the fragments generated from the central region (Q^{54}–P^{122}) appeared only after 3 or 5 h. In *High Phosphates* composition no cleavage site was observed in the central region (Q^{54}–P^{146}), which also showed the slowest cleavage rate with the maximum accumulation of rH163 at 4 hour time-point (Fig. 1E). In a similar manner, in the *No Calcium and Phosphates* composition, where the accumulation of rH163 reached the maximum amount at 1 h (Fig. 1A), the cleavage site in the central region (Q^{54}–P^{146}) appeared only after 5 h. Under conditions of the *High Calcium* composition, where the fastest cleavage rate was observed, few exclusive and additional cleavage sites at T^{61}, H^{67} and H^{130} were also observed. Other conditions also showed some exclusive cleavage sites such as P^{2} for *No Calcium and Phosphates*, P^{50} for *Low Calcium and Phosphates* and G^{10} for *High Calcium and Phosphates*. The N-terminal positions –Y^{11}, N^{13}, F^{14}, S^{15}, E^{17}, K^{23}, W^{24}, P^{33}, G^{42}, and S^{53}; and the C-terminal positions – P^{155} and T^{158} were cleaved in all compositions used. However, peptides originating at position P^{163} were not observed in any compositions, in spite of the appearance of rH163. Possibly, the fragment was readily further cleaved into di- and/or tripeptides whose sizes were below MS acquisition range and hence were not detected, as reported by Ryu et al. [26]. The other major fragment (m/z of 14,843) shown in MALDI besides rH163 and rH146 was identified as Y^{25}–P^{155}.

3.4. Effect of mineral ions on particle size

Various mineral ion compositions were examined to assess the effects of mineral ions on particle size (Fig. 4). The effects were diverse in all the conditions used and did not show any consistent trends. In the *No Calcium and Phosphates* composition the particle diameter increased from 10–20 nm to 3000 nm in 1.5 h and after that it began to decrease (Fig. 4A); and the size increase coincided with the accumulation of rH163 as observed during cleavage (Fig. 1A). In the *Low Calcium and Phosphate* composition, particle sizes (10–20 nm) remained unchanged at all the time-points (Fig. 4B) but in the *High Calcium and Phosphates* composition, particle size increased in a few minutes from 10 to 20 nm and from 800 to 1000 nm and then decreased to ≈500 nm (Fig. 4C). The effect on particle size in the *High Phosphates* composition (Fig. 4E) also coincided with the accumulation of rH163 (Fig. 1E). In both cases the maximum of rH163 concentration appeared after 4 h. In *High Calcium* composition, aggregation was observed instantly and particle size exceeded the detectable limit of the instrument (6000 nm) in a few minutes (Fig. 4D); however, at such high

concentration of calcium and phosphates, mineral may be formed thus contributing to the light scattering.

4. Discussion

The full-length native amelogenin is secreted as 175 amino acid protein in human [31] and 173 in pig [32], and accompanied by various alternatively spliced forms like LRAP [32]. Importantly, the expression of full length amelogenin in the developing matrix is ephemeral as the full length protein is readily processed by MMP-20 into various smaller fragments ranging from 3.5 to 19.5 kDa [26,33]. Some of these fragments have been studied in detail and found to be biologically relevant [1,6,9,11,16]. Since amelogenins show high level of sequence conservation among different mammalian species [34] and similar cleavage patterns by MMP-20 proteolysis from diverse sources have been reported [25,26,33], a comparative account, among all mammalian species can be assumed biologically relevant.

In the present investigation, human amelogenin rH174 was cleaved with MMP-20 in the presence of various compositions of mineral ions calcium (Ca^{2+}) and phosphates ($H_xPO_4^{x-3}$). In general, cleavage at the sites reported earlier [8,25,26] with some additional ones was observed with a clear impact of specific conditions on site preference and time lag for the cleavage. Among major *in vivo* reported fragments, 23 kDa (M^1–P^{163}) and 20 kDa (M^1–P^{146}) [14,35] were detected in SDS page but interestingly the two major reported fragments, TRAPs [9] and 13 kDa [10] were not detected probably due to rapid cleavage of these fragments into smaller ones in present sets of condition. Furthermore, even cleavage before L^{44} required to produce the equivalent 13 kDa fragment [8] (L^{44}–P^{146} in this case) was not observed in selected experimental conditions (Fig. 3).

Regulation of biomineralization by enzymatic cleavage of matrix proteins appears to be a common principle in bone and dentin formation [36,37]. Enzymatic control over initiation of crystallization results in delaying mineral formation and prevents immediate precipitation of mineral at the moment of secretion which would be detrimental to cell survival or structure development.

In the developing enamel matrix, variation in the mineral ion concentration may be related to ion transport and immobilization onto the growing hydroxyapatite crystal that may in turn affect processing of amelogenin. In the mineral compositions used, accumulation of rH146 (20 kDa) was observed only at *High Calcium and Phosphates* concentrations, but not in other compositions indicating that the precipitation of mineral during proteolysis affects the cleavage pattern, suggesting that the presence of mineral may protect rH146 from further processing by MMP-20. This is in agreement with the observation that this 20 kDa fragment of amelogenin is the most abundant and stable amelogenin form in the enamel matrix [35,38]. In other compositions except *High Calcium*, fair accumulation of rH163 was observed. It appears, as reported for *in vivo* conditions [33], that there are multiple rapid cleavages at the last few amino acid positions (the equivalent position in rH174 would be after residue A^{161}, P^{163}, T^{165} and E^{172}) which likely result in generation of small peptides not detectable by LC–MS/MS, leading to the detection of no cleavages at the C-terminal after A^{161} during the present experiments.

The mineral ions can modulate conformation of either amelogenin or MMP-20 or both in such a way that in certain conditions certain sites are more or less accessible to the catalytic site, or minerals may selectively bind to amelogenin to protect or expose certain sites for MMP-20 cleavage. However, low efficiency of the MMP-20 at high phosphate concentration could also be due to chelating properties of phosphate ions that may withdraw essential calcium and zinc from the catalytic site. It was reported that the hydroxyapatite selectively absorbs amelogenin [39] and may decrease its availability to MMP-20 [28]. If this observation is extended to the present investigation, existence of similar situation in *High Calcium and Phosphates* composition may result in formation of some hydroxyapatite, which may lead to the slowest activity of MMP-20 in this condition.

Our experiments revealed some novel albeit unexpected observations. It was reported earlier that the removal of the C-terminus reduces the ability of the amelogenin to interact with hydroxyapatite [40]. This notion was further supported by SSNMR studies where charged C-terminus in LRAP was found to be oriented towards the hydroxyapa-tite surface [41] and by the results of fluorescence spectroscopy that elaborates the affinity of calcium and phosphate for C-termini [42]. Therefore, we expected that C-terminus should be more resistant to proteolysis in *High Calcium and Phosphates*. However, the contrary results were observed as few additional cleavage sites appeared in C-terminus at L^{159}, E^{160} and A^{161}. It suggests that once amelogenin is cleaved at the central region, the C-terminus is no longer protected against proteolysis.

In the kinetic experiments, the MMP-20 appeared to be fastest and most efficient at *High Calcium* composition, and slowest and least efficient at *High Phosphates* and *High Calcium and Phosphates* composition. The kinetic parameters (K_{cat} and K_{cat}/K_m) determined for MMP-20 using fluorescence-quenched peptide as substrate [25] were higher by two orders of magnitude from those reported here for the natural amelogenin. In comparison to other proteases, the efficiency of MMP-20 is equal to that of pepsin but is two orders higher than that of chymotrypsin [43].

The present investigation enumerates the possibilities of the processing of amelogenin by MMP-20 in a developing matrix where changes in concentration of mineral ions will control the process in a highly dynamic fashion. The results indicate the importance of selecting proper physicochemical conditions, while investigating the hydrolysis of amelogenin *in vitro*. This is also in agreement with recent observations on the effect of physical chemistry that exerts on self-assembly of amelogenin, where the presence of calcium and phosphate completely alters amelogenin supramolecular structures [5].

Such parameters will also be critical when attempts are made to mimic enamel growth or to synthesize an enamel-like material *in vitro*. Furthermore, this study suggests that under conditions of calcium deficiency in a growing tooth, amelogenin can be digested prematurely and non-specifically leading to poor enamel synthesis.

In conclusion, MMP-20 was found to behave like a low fidelity enzyme at pH 7.4, whose site preference could be altered by mineral ions that can alter either the enzyme or the substrate conformation or both of them. How these effects are manifested: (1) by change in

enzyme or substrate conformations or (2) by binding of mineral ions to the substrate or (3) by masking the catalytic or cleavage site by mineral ions *etc.*, remains an open question for future studies. Calcium and phosphate concentrations in the enamel matrix have been reported to be around 0.5–1.0 mM and 3.0–6.0 mM, respectively [44], which may also be much higher since an amorphous calcium phosphate (ACP) mineral phase has been observed that may act as a precursor to apatite formation [45]. Water removal from the enamel matrix is required for the formation of ACP, resulting in a gradual increase in the concentration of mineralizing ions during enamel maturation. This study shows that MMP-20s activity can be modulated by the concentration of calcium and phosphate ions when attempting to simulate amelogenin processing *in vitro*. This study also reveals that altered physicochemical conditions can have serious consequences in amelogenin removal and may lead to malformation of tooth enamel. It will be of future interest to evaluate the effects of deficiency or excess of calcium and phosphates in diet using suitable animal models to ascertain the validity of these *in vitro* studies.

Supplementary Material

Refer to Web version on PubMed Central for supplementary material.

Acknowledgments

We thank Ms Grace Nomomura for technical support during the experimentation. These studies were supported by NIH/NIDCR grants DE-RO1-017529, RO1-017529S2, 2R01DE015821 and 3R01DE015821S1. The UCSF Sandler-Moore Mass Spectrometry Core Facility acknowledges support from the Sandler Family Foundation, the Gordon and Betty Moore Foundation, NIH/NCI Cancer Center Support Grant P30 CA082103 and the Office of Science, Office of Biological and Environmental Research of the U.S. Department of Energy under contract no. DE-AC02-05CH11231.

References

1. Fincham AG, Moradian-Oldak J, Simmer JP. The structural biology of the developing dental enamel matrix. J Struct Biol. 1999; 126:270–299. [PubMed: 10441532]
2. Moradian-Oldak J. Amelogenins: assembly, processing and control of crystal morphology. Matrix Biol. 2001; 20:293–305. [PubMed: 11566263]
3. Martinez-Avila O, Wu S, Cheng Y, Lee R, Khan F, Habelitz S. Self-assembly of amelogenin proteins at the water–oil interface. Eur J Oral Sci. 2011; 119:75–82. [PubMed: 22243231]
4. Martinez-Avila OM, Wu S, Kim SJ, Chen Y, Samudrala R, Khan F, Sali A, Horst JA, Habelitz S. Self-assembly of filamentous amelogenin requires calcium and phosphate: from dimers via nanoribbons to fibrils. Biomacromolecules. 2012; 13:3494–3502. [PubMed: 22974364]
5. He X, Wu S, Martinez-Avila O, Cheng Y, Habelitz S. Self-aligning amelogenin nanoribbons in oil–water system. J Struct Biol. 2011; 174:203–212. [PubMed: 21134461]
6. Uskokovic V, Castiglione Z, Cubas P, Zhu L, Li W, Habelitz S. Zeta-potential and particle size analysis of human amelogenins. J Dent Res. 2010; 89:149–153. [PubMed: 20040742]
7. Llano E, Pendas AM, Knauper V, Sorsa T, Salo T, Salido E, Murphy G, Simmer JP, Bartlett JD, Lopez-Otin C. Identification and structural and functional characterization of human enamelysin (MMP-20). Biochemistry. 1997; 36:15101–15108. [PubMed: 9398237]
8. Nagano T, Kakegawa A, Yamakoshi Y, Tsuchiya S, Hu JCC, Gomi K, Arai T, Bartlett JD, Simmer JP. Mmp-20 and Klk4 cleavage site preferences for amelogenin sequences. J Dent Res. 2009; 88:823–828. [PubMed: 19767579]
9. Fincham AG, Hu YY, Pavlova Z, Slavkin HC, Snead ML. Human amelogenins: sequences of “TRAP” molecules. Calcif Tissue Int. 1989; 45:243–250. [PubMed: 2509010]

10. Yeh JH, Takagi T, Sasaki S. Isolation of two bovine amelogenin peptides and their amino acid sequences. Adv Dent Res. 1987; 1:276–281. [PubMed: 3504176]
11. Fukae M, Shimizu M. Amino acid sequence of the main component of porcine enamel proteins. Jpn J Oral Biol. 1983; 25(Suppl):29.
12. Kim JW, Simmer JP, Hart TC, Hart PS, Ramaswami MD, Bartlett JD, Hu JC. MMP-20 mutation in autosomal recessive pigmented hypomaturation amelogenesis imperfecta. J Med Genet. 2005; 42:271–275. [PubMed: 15744043]
13. Hart PS, Hart TC, Michalec MD, Ryu OH, Simmons D, Hong S, Wright JT. Mutation in kallikrein 4 causes autosomal recessive hypomaturation amelogenesis imperfecta. J Med Genet. 2004; 41:545–549. [PubMed: 15235027]
14. Bartlett JD, Simmer JP. Proteinases in developing dental enamel. Crit Rev Oral Biol Med. 1999; 10:425–441. [PubMed: 10634581]
15. Zhu L, Tanimoto K, Le T, DenBesten PK, Li W. Functional roles of prolines at amelogenin C terminal during tooth enamel formation. Cells Tissues Organs. 2009; 189:203–206. [PubMed: 18701806]
16. He X, Li W, Habelitz S. The cooperative self-assembly of 25 and 23 kDa amelogenins. J Struct Biol. 2008; 164:314–321. [PubMed: 18845261]
17. Snead ML. Amelogenin protein exhibits a modular design: implications for form and function. Connect Tissue Res. 2003; 44(Suppl 1):47–51. [PubMed: 12952173]
18. Ozdemir D, Hart PS, Ryu OH, Choi SJ, Ozdemir-Karatas M, Firatli E, Piesco N, Hart TC. MMP20 active-site mutation in hypomaturation amelogenesis imperfecta. J Dent Res. 2005; 84:1031–1035. [PubMed: 16246936]
19. Caterina JJ, Skobe Z, Shi J, Ding Y, Simmer JP, Birkedal-Hansen H, Bartlett JD. Enamelysin (matrix metalloproteinase 20)-deficient mice display an amelogenesis imperfecta phenotype. J Biol Chem. 2002; 277:49598–49604. [PubMed: 12393861]
20. Birkedal-Hansen H, Moore WG, Bodden MK, Windsor LJ, Birkedal-Hansen B, DeCarlo A, Engler JA. Matrix metalloproteinases: a review. Crit Rev Oral Biol Med. 1993; 4:197–250. [PubMed: 8435466]
21. Palosaari H, Pennington CJ, Larmas M, Edwards DR, Tjaderhane L, Salo T. Expression profile of matrix metalloproteinases (MMPs) and tissue inhibitors of MMPs in mature human odontoblasts and pulp tissue. Eur J Oral Sci. 2003; 111:117–127. [PubMed: 12648263]
22. Bartlett JD, Simmer JP, Xue J, Margolis HC, Moreno EC. Molecular cloning and mRNA tissue distribution of a novel matrix metalloproteinase isolated from porcine enamel organ. Gene. 1996; 183:123–128. [PubMed: 8996096]
23. Bartlett JD, Ryu OH, Xue J, Simmer JP, Margolis HC. Enamelysin mRNA displays a developmentally defined pattern of expression and encodes a protein which degrades amelogenin. Connect Tissue Res. 1998; 39:101–109. [PubMed: 11062992]
24. Den Besten PK, Punzi JS, Li W. Purification and sequencing of a 21 kDa and 25 kDa bovine enamel metalloproteinase. Eur J Oral Sci. 1998; 106 (Suppl 1):345–349. [PubMed: 9541246]
25. Zhu L, Tanimoto K, Robinsin S, Chen J, Witkowska E, Hall S, Le T, DenBesten PK, Li W. Comparative properties of recombinant human and bovine matrix metalloproteinase-20. Arch Oral Biol. 2008; 53:785–790. [PubMed: 18336793]
26. Ryu OH, Fincham AG, Hu CC, Zhang C, Qian Q, Bartlett JD, Simmer JP. Characterization of recombinant pig enamelysin activity and cleavage of recombinant pig and mouse amelogenins. J Dent Res. 1999; 78:743–750. [PubMed: 10096449]
27. Sun Z, Fan D, Fan Y, Du C, Moradian-Oldak J. Enamel proteases reduce amelogenin-apatite binding. J Dent Res. 2008; 87:1133–1137. [PubMed: 19029081]
28. Sun Z, Carpiaux W, Fan D, Fan Y, Lakshminarayanan R, Moradian-Oldak J. Apatite reduces amelogenin proteolysis by MMP-20 and KLK4 in vitro. J Dent Res. 2010; 89:344–348. [PubMed: 20160068]
29. Uskokovic V, Khan F, Liu H, Witkowska HE, Zhu L, Li W, Habelitz S. Hydrolysis of amelogenin by matrix metalloprotease-20 accelerates mineralization in vitro. Arch Oral Biol. 2011; 56:1548–1559. [PubMed: 21774914]

30. Li W, Gao C, Yan Y, DenBesten P. X-linked amelogenesis imperfecta may result from decreased formation of tyrosine rich amelogenin peptide (TRAP). Arch Oral Biol. 2003; 48:177–183. [PubMed: 12648554]
31. Salido EC, Yen PH, Koprivnikar K, Yu LC, Shapiro LJ. The human enamel protein gene amelogenin is expressed from both the X and the Y chromosomes. Am J Hum Genet. 1992; 50:303–316. [PubMed: 1734713]
32. Hu CC, Bartlett JD, Zhang CH, Qian Q, Ryu OH, Simmer JP. Cloning, cDNA sequence, and alternative splicing of porcine amelogenin mRNAs. J Dent Res. 1996; 75:1735–1741. [PubMed: 8955667]
33. Fincham AG, Moradian-Oldak J. Comparative mass spectrometric analyses of enamel matrix proteins from five species suggest a common pathway of post-secretory proteolytic processing. Connect Tissue Res. 1996; 35:151–156. [PubMed: 9084653]
34. Takagi T, Suzuki M, Baba T, Minegishi K, Sasaki S. Complete amino acid sequence of amelogenin in developing bovine enamel. Biochem Biophys Res Commun. 1984; 121:592–597. [PubMed: 6732825]
35. Yamakoshi Y, Tanabe T, Fukae M, Shimizu M. Porcine amelogenins. Calcif Tissue Int. 1994; 54:69–75. [PubMed: 8118757]
36. Butler WT, Brunn JC, Qin C. Dentin extracellular matrix (ECM) proteins: comparison to bone ECM and contribution to dynamics of dentinogenesis. Connect Tissue Res. 2003; 44(Suppl 1): 171–178. [PubMed: 12952193]
37. George A, Veis A. Phosphorylated proteins and control over apatite nucleation, crystal growth, and inhibition. Chem Rev. 2008; 108:4670–4693. [PubMed: 18831570]
38. Tanabe T, Fukae M, Uchida T, Shimizu M. The localization and characterization of proteinases for the initial cleavage of porcine amelogenin. Calcif Tissue Int. 1992; 51:213–217. [PubMed: 1422965]
39. Aoba T, Fukae M, Tanabe T, Shimizu M, Moreno EC. Selective adsorption of porcine-amelogenins onto hydroxyapatite and their inhibitory activity on hy-droxyapatite growth in supersaturated solutions. Calcif Tissue Int. 1987; 41:281–289. [PubMed: 2825935]
40. Moradian-Oldak J, Bouropoulos N, Wang L, Gharakhanian N. Analysis of self-assembly and apatite binding properties of amelogenin proteins lacking the hydrophilic C-terminal. Matrix Biol. 2002; 21:197–205. [PubMed: 11852235]
41. Shaw WJ, Campbell AA, Paine ML, Snead ML. The COOH terminus of the amelogenin, LRAP, is oriented next to the hydroxyapatite surface. J Biol Chem. 2004; 279:40263–40266. [PubMed: 15299015]
42. Khan F, Li W, Habelitz S. Biophysical characterization of synthetic amelogenin C-terminal peptides. Eur J Oral Sci. 2012; 120:113–122. [PubMed: 22409217]
43. Mathews, CK.; Van Holde, KE.; Ahern, KG. Biochemistry. Benjamin Cumming; San Francisco: 2000.
44. Aoba T, Moreno EC. The enamel fluid in the early secretory stage of porcine amelogenesis: chemical composition and saturation with respect to enamel mineral. Calcif Tissue Int. 1987; 41:86–94. [PubMed: 3115550]
45. Beniash E, Metzler RA, Lam RS, Gilbert PU. Transient amorphous calcium phosphate in forming enamel. J Struct Biol. 2009; 166:133–143. [PubMed: 19217943]

Appendix A. Supplementary data

Supplementary data to this article can be found online at http://dx.doi.org/10.1016/j.bbagen.2012.11.021.

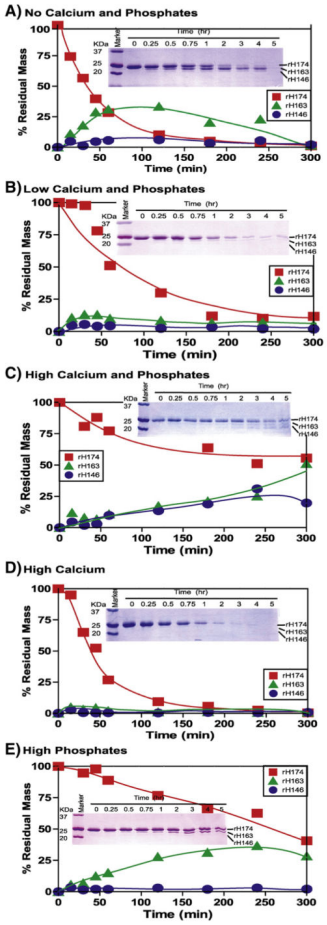

Fig. 1.

Time-dependent proteolytic course of amelogenin (rH174) by MMP-20 at different mineral ion compositions. The substrate (rH174) (50.5 μM) was cleaved by MMP-20 (0.16 μM) and during the time course the substrate and products were visualized by SDS-PAGE (inset) and their quantities are plotted against time. Reactions were carried out in 10 mM Tris buffer, 50 mM KCl, 1 μM $ZnCl_2$, and 60 μM $CaCl_2$ at pH 7.4 with the addition of $CaCl_2$ and KH_2PO_4. (A) *No Calcium and Phosphates* – no extra $CaCl_2$ or KH_2PO_4 added, except 60 μM $CaCl_2$ already present in buffer; (B) *Low Calcium and Phosphates* – 3.34 mM $CaCl_2$ and 2.09 mM KH_2PO_4; (C) *High Calcium and Phosphates* –33.4 mM $CaCl_2$ and 20.9 mM KH_2PO_4; (D) *High Calcium* – 33.4 mM $CaCl_2$; (E) *High Phosphates* – 20.9 mM KH_2PO_4.

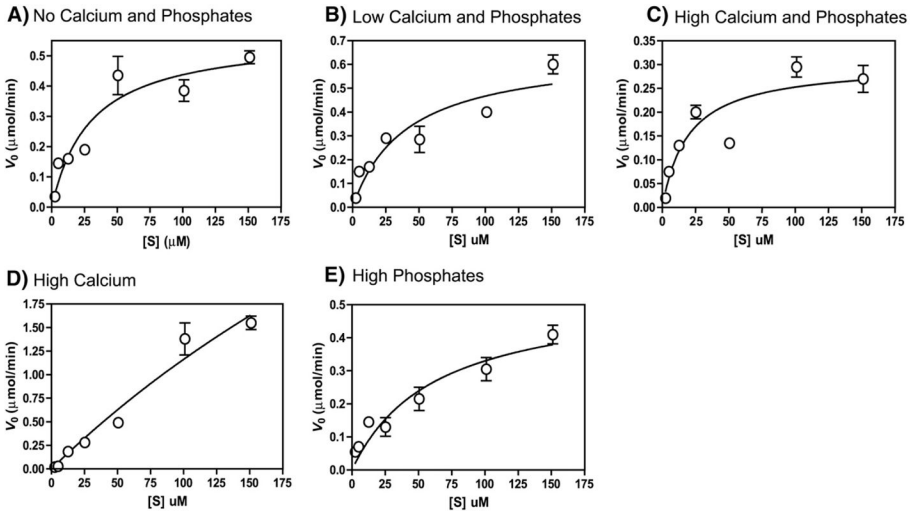

Fig. 2.

Steady state kinetics of MMP-20 cleaving substrate (amelogenin). Various concentrations of amelogenin (2.5–151 μM) were incubated with 0.16 μM of MMP-20 at 37 °C in a reaction buffer consisting of 10 mM Tris buffer, 50 mM KCl, 1 μM $ZnCl_2$, and 60 μM $CaCl_2$ at pH 7.4 with the following composition of mineral ions – (A) *No Calcium and Phosphates* – no extra $CaCl_2$ or KH_2PO_4 added, except 60 μM $CaCl_2$ already present in buffer; (B) *Low Calcium and Phosphates* – 3.34 mM $CaCl_2$ and 2.09 mM KH_2PO_4; (C) *High Calcium and Phosphates* – 33.4 mM $CaCl_2$ and 20.9 mM KH_2PO_4; (D) *High Calcium* – 33.4 mM $CaCl_2$; and (E) *High Phosphates* – 20.9 mM KH_2PO_4. Initial reaction velocity (v_0) was determined before less than 10% of the substrate was consumed and plotted as a function of respective substrate concentration. Data were fitted to the Michaelis–Menten equation by non-linear regression.

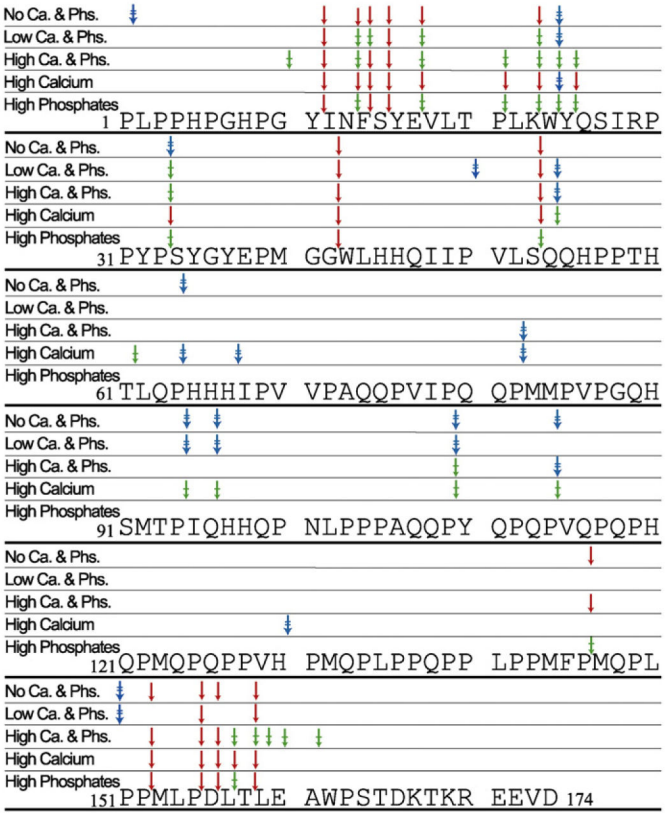

Fig. 3.

The amelogenin sequence showing MMP-20 cleavage sites at various mineral ion compositions. The fragments after 1, 3 and 5 h were identified by MALDI-LC-MS/MS and the related cleavage position are marked – after 1 h (↓; red), 3 h (↕; green), and 5 h (↯; blue).

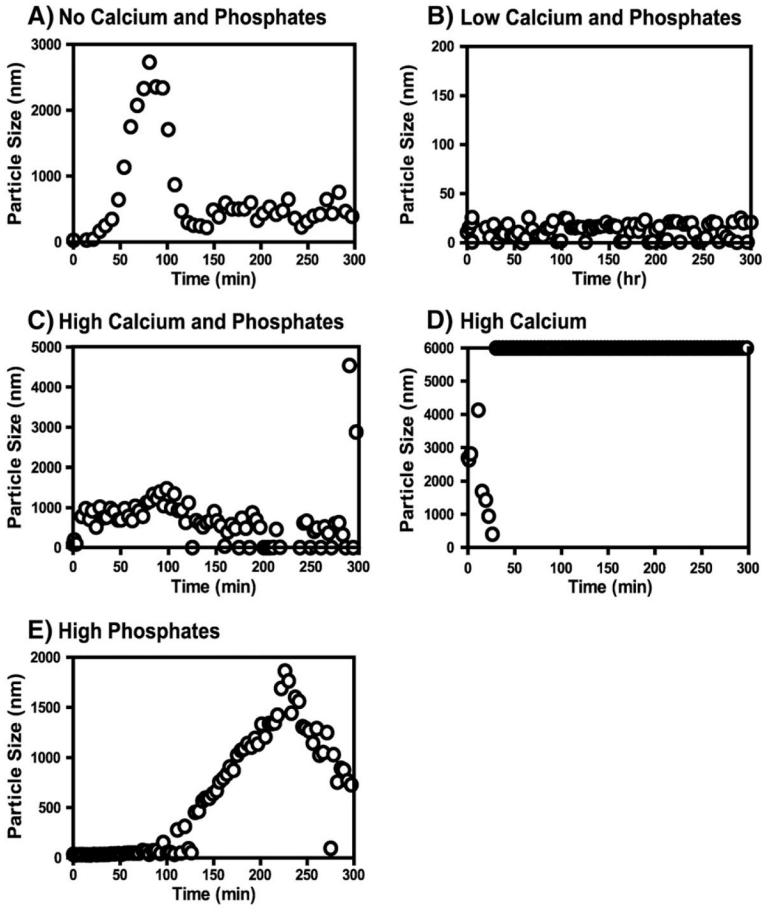

Fig. 4.

The average particle size of amelogenin during the cleavage time-course by MMP-20 in various mineral ion compositions. The particle size 6000 nm is the saturation limit of the instrument, data at this point data represent particles of equal and larger than 6000 nm. (A) *No Calcium and Phosphates*; (B) *Low Calcium and Phosphates*; (C) *High Calcium and Phosphates*; (D) *High Calcium*; (E) *High Phosphates*.

Table 1

Kinetic parameters of MMP-20 binding to and hydrolysis of rH174.

Mineral ion concentration	V_{max} **(μM/min)**	K_m **(μM)**	K_{cat} **(1/s)**	K_{cat}/K_m **(×10^3 M^{-1} s^{-1})**	k **(×10^{-5}1/s)**	$T_{1/2}$ **(min)**
No Calcium and Phosphates[1]	0.56 (±0.06)	29.90 (±9.6)	0.058	1.9	24.5 (0.97)	47
Low Calcium and Phosphates[2]	0.66 (±0.09)	40.70 (±15.2)	0.068	1.6	15.8 (0.98)	73
High Calcium[3]	7.5 (±5.8)	584.6 (±489)	0.77	1.3	32.9 (0.99)	35
High Phosphates[4]	0.54 (±0.06)	63.39 (±20.8)	0.056	0.8	3.21 (0.91)	370
High Calcium and Phosphates[5]	0.30 (±0.03)	19.51 (±7.3)	0.031	1.6	5.01 (0.92)	227

The cleavage reactions were carried at protein concentrations 50.5 μM rH174 and 0.16 μM MMP-20 in a reaction buffer consists of 10 mM Tris buffer, 50 mM KCl, 1 μM $ZnCl_2$, and 60 μM $CaCl_2$, pH 7.4 at 37 °C, with the following minerals:

[1] *No Calcium and Phosphates*=0 M $CaCl_2$ and 0 M KH_2PO_4 (contains 60 μM $CaCl_2$ already in buffer);

[2] *Low Calcium and Phosphates*=3.34 mM $CaCl_2$ and 2.29 mM KH_2PO_4;

[3] *High Calcium*=33.4 mM $CaCl_2$;

[4] *High Phosphates*=22.9 mM KH_2PO_4; and

[5] *High Calcium and Phosphates*=33.4 mM $CaCl_2$ and 22.9 mM KH_2PO_4.

Value in parentheses is Std. Error for V_{max} and K_m, and $R2$ for k.